J. Fluid Mech. (1988), *vol.* 196, *pp.* 409–430
Printed in Great Britain

Viscoelastic response of a floating ice plate to a steadily moving load

By R. J. HOSKING,† A. D. SNEYD AND D. W. WAUGH
Mathematics Department, University of Waikato, Hamilton, New Zealand

(Received 18 September 1987)

Viscoelastic theory is used to describe the response of a floating ice sheet to a moving vehicle. We adopt a two-parameter memory function to describe the behaviour of the ice, subjected to a steadily moving line or point load. The viscoelastic dissipation produces an asymmetric quasi-static response at subcritical speed, renders a finite response at the critical speed, and damps the shorter leading waves rather more severely than the longer trailing waves at supercritical speed. We extend earlier asymptotic theory to consider the anisotropic damping of the flexural waves. There is enhanced agreement between theory and experiment.

1. Introduction

Many features of the response of a floating ice sheet to a moving vehicle can be explained by modelling the ice as a thin elastic plate. Wilson (1958) observed that flexural waves occur if the load speed V exceeds the local minimum $c_{\min}$ of a classical elastic-gravity free wave dispersion relation (Greenhill 1887), whereas at lower speeds there is a quasi-static response relative to the load resembling that produced when the load is stationary. Theoretical expressions for the ice displacement were first derived by Kheisin (1963) for a steadily moving point or line load. The amplified response at the critical speed $V = c_{\min}$ corresponds to an accumulation of energy underneath the source, since $c_{\min}$ coincides with the group speed (Davys, Hosking & Sneyd 1985). More recent experimental studies of ice waves (Eyre 1977; Beltaos 1981; Takizawa 1985, 1986; Squire *et al.* 1985, 1986) have largely confirmed theoretical predictions obtained assuming a thin elastic plate (cf. Kerr 1983; Hosking & Sneyd 1986; Schulkes, Hosking & Sneyd 1987; Schulkes & Sneyd 1988). Reference may also be made to a survey by Kerr (1981).

There are however certain features that are not satisfactorily described by the elastic theory, such as the observed lag of the position of maximum depression immediately behind the source (Takizawa 1985). Given earlier analysis for the simpler problem of a beam resting on an elastic foundation, this phenomenon is probably due to dissipation (cf. Kerr 1981; Takizawa 1986). We are also interested in the viscoelastic damping of flexural waves with distance from the source (Davys *et al.* 1985). In this paper, we modify the mathematical model for the ice plate to consider viscoelasticity, and find that both phenomena can be well understood using a simple memory function involving two viscoelastic parameters. The viscoelastic equation of motion is discussed in §2, followed by analysis for a steadily moving line source in §3, and for a point source in §4. We give results for parameters typical of McMurdo Sound (Antarctica) in this discussion, but in §5 we also briefly consider the relevant experimental data obtained by Takizawa (1985, 1986) in Japan.

† New address: Department of Mathematics, James Cook University, Townsville Q4811, Australia.

2. Viscoelastic equation of motion

Consider an infinite homogeneous ice sheet of thickness h and density ρ_i, floating on water of density ρ. The undisturbed water surface is at $z = 0$ and the sea bed at $z = -H$, as shown in figure 1. If $\eta(x, y, t)$ represents a small vertical ice-sheet deflection, then the equation of motion for the ice sheet treated as an elastic plate is

$$D\nabla^4\eta + \rho_i h\eta_{tt} = p - f(x, y, t), \tag{2.1}$$

where

$$D = \frac{Eh^3}{12(1-\nu^2)}. \tag{2.2}$$

Here, E denotes Young's modulus and ν Poisson's ratio for ice, p is the water pressure at $z = 0$, and $f(x, y, t)$ is the loading function, or downward stress exerted on the ice due to the load. Typical figures for McMurdo Sound are $E = 5 \times 10^9\ \mathrm{Nm}^{-2}$, $h = 2.5$ m, $H = 350$ m and $\nu = \frac{1}{3}$ (cf. Davys *et al.* 1985), which we again adopt in this paper unless otherwise stated. Introducing viscoelasticity modifies the bending-force term $f_B = D\nabla^4\eta$ in (2.1). Since we are concerned with only very small ice deflections due to a moving load, we adopt a linear viscoelastic model where

$$f_B(x, y, t) = D\nabla^4\left[\eta(x, y, t) - \int_0^\infty \Psi(\tau)\,\eta(x, y, t-\tau)\,\mathrm{d}\tau\right],$$

corresponding to a constitutive equation involving an hereditary integral (Boltzmann 1874; Graffi 1982). The function $\Psi(t)$ is called a memory function, for now the bending force depends not only on the instantaneous deformation but also the deformation history. We assume that the memory of the ice fades with time (this is in agreement with the fading memory hypothesis of Coleman & Noll 1961), so that $|\Psi(t)|$ decreases monotonically to zero as $t \to \infty$. If we assume a general relationship between the bending force f_B and the displacement η of the form

$$\sum_{k=0}^{n} a_k \frac{\partial^k}{\partial t^k} f_B = \sum_{k=0}^{n} b_k \frac{\partial^k}{\partial t^k} \nabla^4\eta,$$

it follows that the memory function is represented by a finite sum of exponentials (cf. Graffi 1982), i.e.

$$\Psi(t) = \sum_{j=0}^{n} A_j \mathrm{e}^{-\alpha_j t}, \tag{2.3}$$

where the A_j and α_j are viscoelastic parameters. For $\Psi(t)$ to satisfy the fading-memory hypothesis it is necessary that each $\alpha_j > 0$ and that all A_j have the same sign. Furthermore, to ensure positive energy dissipation we have that each $A_j > 0$ (cf. Appendix A). Thus the equation of motion of a viscoelastic ice plate is

$$D\nabla^4\left[\eta(x, y, t) - \int_0^\infty \Psi(\tau)\,\eta(x, y, t-\tau)\,\mathrm{d}\tau\right] + \rho_i h\eta_{tt} = p - f(x, y, t). \tag{2.4}$$

Note that this formulation of the viscoelastic equation of motion is equivalent to using the correspondence principle of viscoelasticity (cf. Squire & Allan 1980, Bates & Shapiro 1981*a*, *b*).

Assuming that the sea-water flow is irrotational with velocity potential ϕ, we can use Bernoulli's theorem to rewrite (2.4) as

$$D\nabla^4\left[\eta(x, y, t) - \int_0^\infty \Psi(\tau)\,\eta(x, y, t-\tau)\,\mathrm{d}\tau\right] + \rho_i h\eta_{tt} = -\rho(\phi_t)_{z=0} - \rho g\eta - f(x, y, t). \tag{2.5}$$

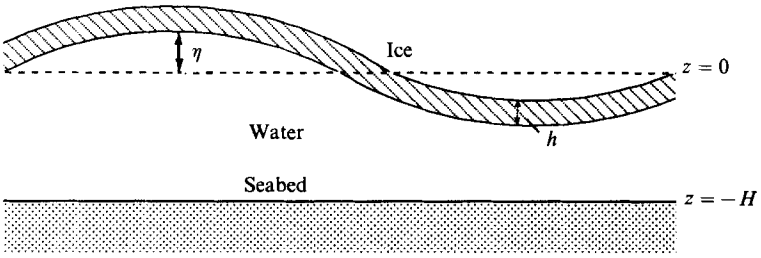

FIGURE 1. Diagram of floating ice plate.

In the following discussion we neglect the acceleration term $\rho_i h\eta_{tt}$, which is justified in our context because the wavelength of the surface displacement is always much larger than the ice thickness h. Since the water motion penetrates to a depth comparable with one wavelength, the inertia of the thin plate is small compared with that of the moving water.

The viscoelastic equation of motion (2.5) may be solved by taking a Fourier transform in x, y and t: thus writing

$$\hat{\eta}(l, m, \omega) = (2\pi)^{-\frac{3}{2}} \int \eta(x, y, t)\, \mathrm{e}^{\mathrm{i}(lx+my-\omega t)}\, \mathrm{d}x\, \mathrm{d}y\, \mathrm{d}t,$$

and assuming that the disturbances vanish at infinity, we obtain

$$\hat{\eta} = \frac{-\hat{f}(l, m, \omega)}{Dk^4(1-\psi)+\rho g-(\rho\omega^2/k)\coth kH}, \tag{2.6}$$

where $k^2 = l^2+m^2$ and

$$\psi(\omega) = \int_0^\infty \Psi(\tau)\, \mathrm{e}^{-\mathrm{i}\omega\tau}\, \mathrm{d}\tau \tag{2.7}$$

defines the parametric frequency dependence introduced by the viscoelasticity. We have used the usual irrotational water-wave theory to evaluate ϕ_t, and note that the elastic limit corresponds to $\psi \equiv 0$ (cf. Davys *et al.* 1985).

We adopt the simplest possible memory function, by setting $n = 0$ in (2.3). We therefore have two viscoelastic parameters, A_0 representing the magnitude of viscoelastic effects, and α_0 the reciprocal of the memory timescale. This is a generalisation of the memory function for the Maxwell viscoelastic model (where $A_0 = \alpha_0$). Equation (2.7) therefore gives the frequency dependence

$$\psi(\omega) = \frac{A_0}{\alpha_0+\mathrm{i}\omega}. \tag{2.8}$$

We emphasize that our approach is phenomenological. The detailed structure of ice, especially sea ice, is complex and its properties vary considerably with depth. Although there is some experimental evidence to suggest a combination Maxwell–Voigt model (Tabata 1958), we find that two parameters are enough to model the observed dissipative features of the ice displacement due to a moving load. The parameters, including D in the otherwise classical differential equation (2.1) for the displacement of a uniform plate, are interpreted as representing gross properties of the ice.

3. Concentrated line load

For a steady one-dimensional (y-independent) load travelling with speed V in the positive x-direction, we have the loading function

$$f(x, t) = F(x - Vt),$$

so using k as the spatial Fourier transform variable we have

$$\hat{f}(k, \omega) = (2\pi)^{\frac{1}{2}}\delta(Vk - \omega)\,\hat{F}(k),$$

where δ is the Dirac delta-function. In particular, for a concentrated line load with $F = f_0\,\delta(x - Vt)$ we have $\hat{F} = f_0/(2\pi)^{\frac{1}{2}}$, so in this case Fourier inversion of (2.5) yields

$$\eta(X) = \frac{-f_0}{2\pi}\int_{-\infty}^{\infty} \frac{e^{-ikX}\,dk}{Dk^4(1-\psi_V)+\rho g-\rho kV^2\coth kH}, \tag{3.1}$$

where $X = x - Vt$ is a coordinate moving with the source and

$$\psi_V \equiv \psi(kV) = A_0/(\alpha_0 + ikV).$$

It is convenient to write the integral (3.1) in dimensionless form. We define a characteristic lengthscale $L = (3D/\rho g)^{\frac{1}{4}} = k_{\min}^{-1}$, where $k_{\min}$ is the wavenumber at which the phase speed achieves its minimum value $c_{\min} = 2(Dg^3/27\rho)^{\frac{1}{8}}$ according to elastic theory, in the case of deep water (cf. Davys *et al.* 1985). We also define a typical timescale $T = L/c_{\min} = \frac{1}{2}(243D/\rho g^5)^{\frac{1}{8}}$, which for the McMurdo Sound parameters is approximately two seconds. Introducing the dimensionless variables $k' = kL$, $\alpha_0' = \alpha_0 T$, $X' = X/L$ and $V' = V/c_{\min}$ the equation (3.1) can therefore be re-expressed (on dropping the primes) as

$$\eta(X) = \frac{-\mathscr{A}}{2\pi}\int_{-\infty}^{\infty} \frac{e^{-ikX}dk}{G(k)}, \tag{3.2}$$

where

$$\mathscr{A} = \frac{3f_0}{\rho g L}, \quad G(k) = B(k) - \epsilon C(k),$$

$$B(k) = k^4 - 4kV^2\coth kH + 3, \quad C(k) = \frac{k^4}{\alpha_0 + ikV}, \quad \epsilon = A_0 T.$$

Note that (3.2) reduces to the equation for the displacement in the elastic limit when $\epsilon = 0$, and when $\epsilon \ll 1$ the term $\epsilon C(k)$ represents a small viscoelastic perturbation from the elastic case. Henceforth k, α_0, X, V, H are dimensionless except where units are specified.

3.1. *Poles in the integrand*

The integral (3.2) may be evaluated using contour integration. If k_0 denotes a root of $B(k)$, and ϵk_1 is a small perturbation from this point due to viscoelasticity, we have

$$B(k) - \epsilon C(k) = \epsilon[k_1 B'(k_0) - C(k_0)] + O(\epsilon^2).$$

Hence provided $B'(k_0) \neq 0$, to first order in ϵ the integrand of (3.2) has poles at

$$k_p = k_0 + \epsilon\frac{C(k_0)}{B'(k_0)} = k_0 + \epsilon\frac{k_0^4(\alpha_0 - ik_0 V)}{B'(k_0)(\alpha_0^2 + k_0^2 V^2)}. \tag{3.3}$$

When $B'(k_0) = 0$, corresponding to the critical point at which the phase speed is

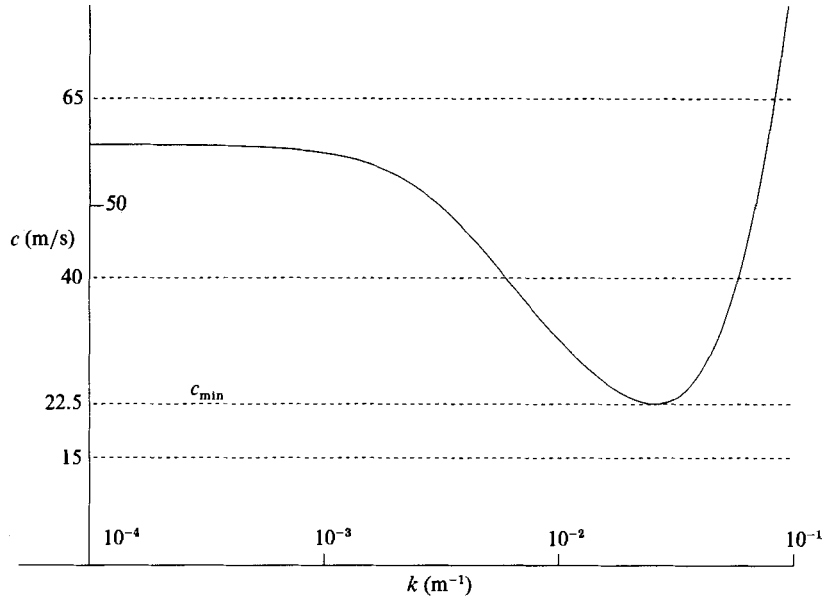

FIGURE 2. Graph of phase speed c against wavenumber k, with reference to vehicle speed.

minimum in the elastic limit (i.e. $V = c_{\min}$), we have to include the next term in the expansion of $B(k)$. The pole then occurs at

$$k_{\mathrm{p}} = k_0 \pm \epsilon^{\frac{1}{2}} \left[\frac{C(k_0)}{B''(k_0)}\right]^{\frac{1}{2}}. \tag{3.4}$$

Note that in this case the perturbation is of order $\epsilon^{\frac{1}{2}}$ rather than ϵ, so the poles are perturbed further as the minimum phase speed is approached.

The function $B(k)$ is even, and for source speeds in the range $c_{\min} < V < (gH)^{\frac{1}{2}}$ has real roots $k_0 = \pm k_y, \pm k_z$ (cf. figure 3) which correspond to the wavenumbers at which the source and phase speeds are equal in the elastic case (cf. figure 2). For $V > (gH)^{\frac{1}{2}}$ the function $B(k)$ has real roots $k_0 = \pm k_z$ only, and when the source speed V is equal to $c_{\min}$ the function $B(k)$ has only two roots, $k_0 = \pm k_{\mathrm{c}}$, which correspond to the critical points at which $B'(k_0) = 0$. Since $C(k)$ is complex the poles k_{p} will be complex – i.e. viscoelasticity moves the poles off the real axis. Since $B'(k)$ is odd, it follows from (3.3) that the viscoelastic perturbation to each pole has an even real part and an odd imaginary part. Thus the poles $\pm k_z$ become $\pm k_1 - \mathrm{i}\delta_1$, and $\pm k_y$ become $\pm k_2 + \mathrm{i}\delta_2$. Note that since $B'(k_y) < 0$ and $B'(k_z) > 0$ (cf. figure 3), we have $k_1 > k_2 > 0$ and $\delta_1, \delta_2 > 0$.

For source speeds less than $c_{\min}$ the function $B(k)$ itself no longer has real roots (cf. figure 3) but complex roots, and since $B(k)$ is a real even function these roots may be written in the form $k_0 = \pm k' \pm \mathrm{i}\delta'$ (cf. figure 4). Equations (3.3) and (3.4) still hold however, so as before the poles of (3.2) may be written in the form

$$k_{\mathrm{p}} = \pm k_1 - \mathrm{i}\delta_1, \ \pm k_2 + \mathrm{i}\delta_2. \tag{3.5}$$

Figure 4 is a plot of the imaginary part of the poles versus the real part, showing that the roots are indeed of the form (3.5), and also that $k_1 > k_2$.

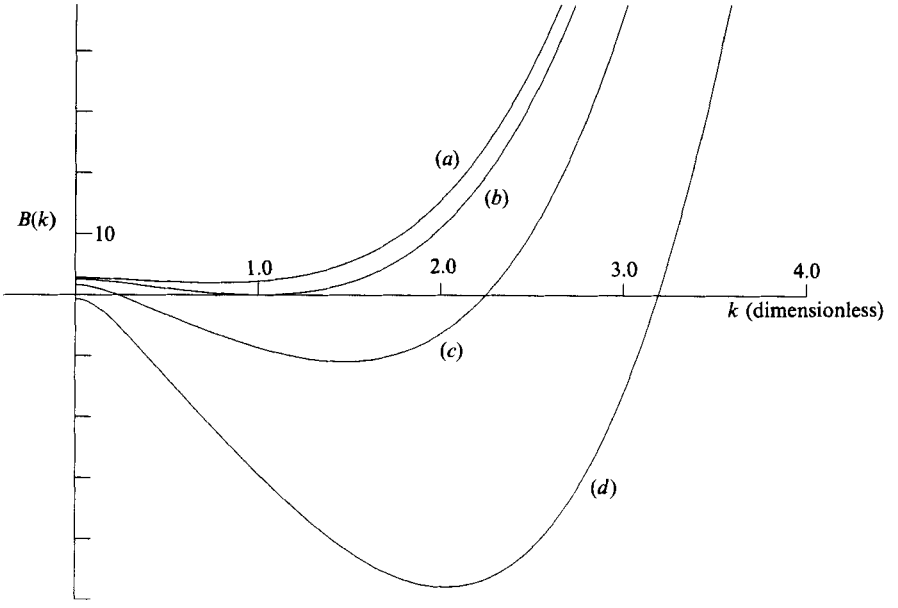

FIGURE 3. Behaviour of elastic component $B(k)$ of dimensionless dispersion relation with source speed (*a*) $V = 15$ m s^{-1}; (*b*) $V = c_{\min} = 22.5$ m s^{-1}; (*c*) $V = 40$ m s^{-1}; (*d*) $V = 65$ m s$^{-1} > (gH)^{\frac{1}{2}}$.

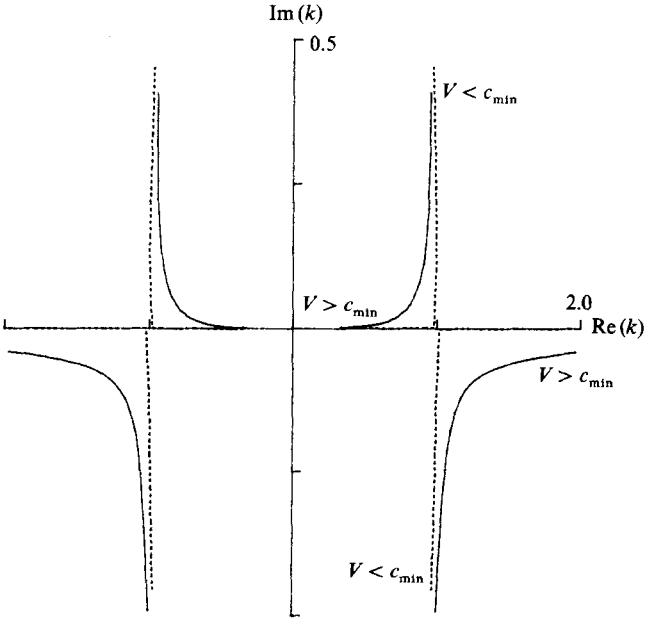

FIGURE 4. Loci of the zeros of the dimensionless dispersion relation, comparing the elastic limit (dashed line) with a viscoelastic case, $A_0 = 0.1$ s^{-1} and $\alpha_0 = 0.1$ s^{-1} (continuous line).

The integrand of (3.2) also has an infinite number of poles on the imaginary axis. If we write $k = is$ and define

$$p(s) = s^4 + 3, \quad q(s) = 4sV^2 \cot sH + \epsilon \frac{s^4}{\alpha_0 - sV},$$

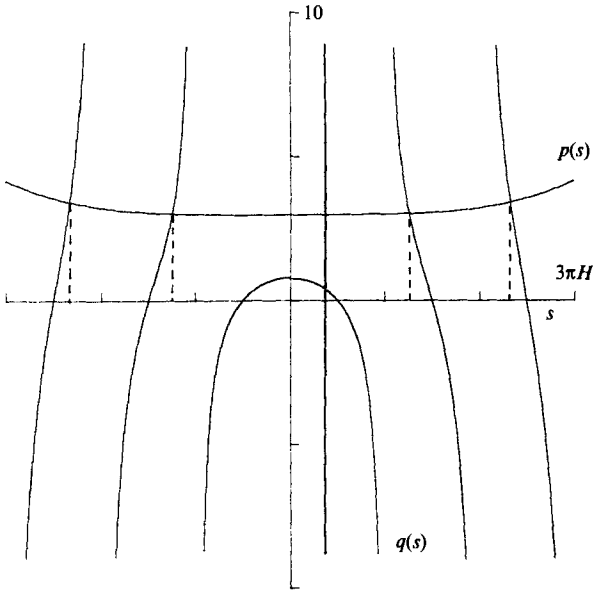

FIGURE 5. Location of the infinite sequence of imaginary poles, at source speed $V = 30$ m s^{-1}. $A_0 = \alpha_0 = 0.1$ s^{-1}.

the points at which $p(s) = q(s)$ correspond to poles in the integrand. Figure 5 shows graphs of the functions p and q, from which we observe a countably infinite sequence of poles at $s_n (n = 1, 2, \ldots)$ where $n\pi/H < s_n < (n+1)\pi/H$, and a similar sequence of poles for s negative. There is also another pole where $s_0 \approx \alpha_0/V$, but no others (cf. Appendix B).

3.2. *Steady displacement*

The steady ice displacement (relative to the source) is given by (3.2), where the integral may be evaluated by contour integration. For $X > 0$ we close the contour by a large semicircle $|k| = R$ in the lower half-plane, along which the integral tends to zero as $R \to \infty$ (by Jordan's lemma). Writing the two poles $k_1 - \mathrm{i}\delta_1$ and $-k_1 - \mathrm{i}\delta_1$ defined previously as k_s and $-\bar{k}_s$ (where $k_s = k_1 - \mathrm{i}\delta_1$), the sum of their residues is

$$\left\{\frac{\mathrm{e}^{-\mathrm{i}k_1 X}}{G'(k_s)} + \frac{\mathrm{e}^{\mathrm{i}k_1 X}}{G'(-\bar{k}_s)}\right\} \mathrm{e}^{-\delta_1 X} = -2\mathrm{i}M_1 \sin(k_1 X + \theta_1)\, \mathrm{e}^{-\delta_1 X},$$

where $M_1 = 1/|G'(k_s)|$ and $\theta_1 = \mathrm{Arg}\{G'(k_s)\}$. For $X < 0$ the contour is closed in the upper half-plane, enclosing poles with positive imaginary part. The poles $\pm k_2 + \mathrm{i}\delta_2$ similarly contribute

$$-2\mathrm{i}M_2 \sin(k_2 X + \theta_2)\, \mathrm{e}^{\delta_2 X}$$

to the displacement η. Only the first few poles in each infinite sequence $\{\pm \mathrm{i}s_n\}$ may give significant contributions to the displacement, and these contributions are only important in the vicinity of the source (cf. Schulkes & Sneyd 1988). The contribution of the pole $\mathrm{i}s_0$ when $X < 0$, which describes the ice memory of the maximum displacement in the vicinity of the source, is $\epsilon M_3 \mathrm{e}^{\alpha_0 X/V}$, where typically $M_3 \ll M_1, M_2$. For larger $|X|$ we therefore have an approximate form for the displacement:

$$\eta = \begin{cases} 2\mathscr{A}M_1 \sin(k_1 X + \theta_1)\, \mathrm{e}^{-\delta_1 X}, & \text{for } X > 0; \\ -2\mathscr{A}M_2 \sin(k_2 X + \theta_2)\, \mathrm{e}^{\delta_2 X}, & \text{for } X < 0. \end{cases} \tag{3.6}$$

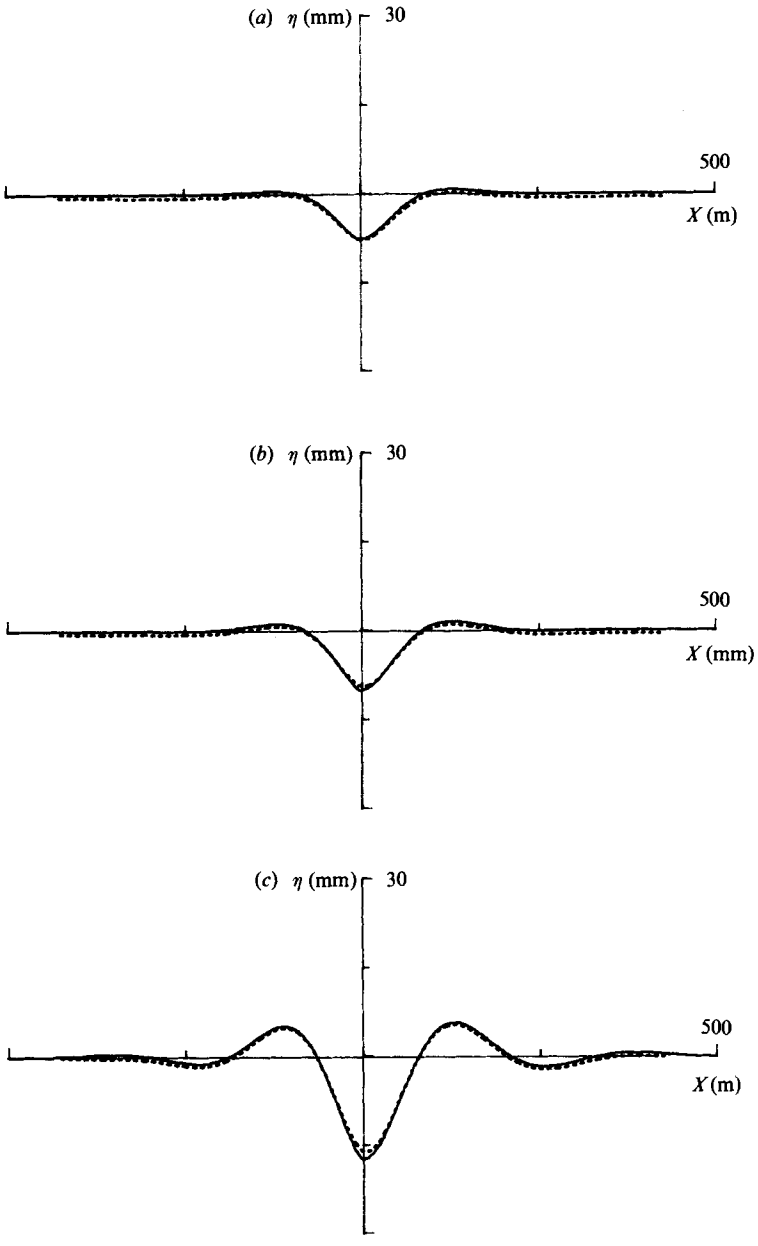

FIGURE 6. Theoretical ice displacements for various subcritical source speeds, to demonstrate the accuracy of the analytical result (3.6) by comparison with calculation using a fast Fourier transform. $A_0 = \alpha_0 = 0.1\ \mathrm{s}^{-1}$. (*a*) $V = 10\ \mathrm{m\ s}^{-1}$, (*b*) 15 m s^{-1}, (*c*) 20 m s^{-1}.

Figure 6(*a–c*) shows the displacement η versus distance X for various subcritical source speeds. The continuous line represents η calculated using (3.6) and the dashed line that calculated using a fast Fourier transform of integral (3.2). Note that the displacement is asymmetric about the origin, rather than symmetric as in the elastic limit (cf. Schulkes & Sneyd 1988). Viscoelasticity causes the point of maximum depression to lag the load (cf. also §4).

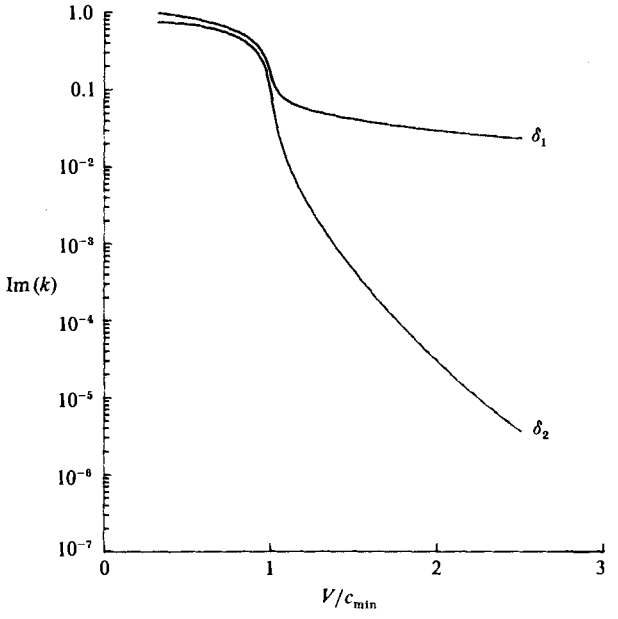

FIGURE 7. Variation of viscoelastic damping coefficients δ_1, δ_2 with source speed. $A_0 = \alpha_0 = 0.1\ \mathrm{s}^{-1}$.

For source speeds exceeding c_{min} we expect waves generated in the ice, with a short wave leading the source and a longer wave trailing it, consistent with our earlier observation that $k_1 > k_2$. From (2.7) we expect the viscoelasticity to more strongly affect the short waves, and we find $\delta_1 \gg \delta_2$ for $V > c_{min}$ (cf. figure 7), so from (3.6) the shorter leading wave is much more strongly damped than the longer trailing wave. Figure 8(*a–c*) shows the ice displacement obtained from (3.6), for a source speed of 30 m s^{-1} (with $c_{min} = 22.5$ m s^{-1}). Figure 8(*a*) shows the displacement for the elastic limit $A_0 = 0$, and as the viscoelastic parameter A_0 increases the waves are damped (cf. figure 8*b*, *c*), with the shorter wave ahead of the source damped considerably more than the longer trailing wave.

Figure 9 shows the response amplitude measure M_1 versus the source speed (scaled to c_{min}) with α_0 fixed while A_0 varies. The significant increase in the displacement amplitude, as the source speed approaches the critical phase speed, resembles that found experimentally (cf. §1). Although the elastic limit is approached as $A_0 \to 0$, we find that the maximum amplitude is *finite* (as previously shown by Bates & Shapiro 1981*a*, *b*), and does not occur exactly at $V = c_{min}$ but at a slightly lower speed. Figure 10 is a similar plot of M_1 versus V/c_{min}, except that now A_0 is fixed and the other viscoelastic parameter α_0 is varied. We note that the maximum amplitude increases as A_0 decreases, and also as α_0 increases – i.e. limiting to the elastic case (as $A_0 \to 0$ or $\alpha_0 \to \infty$). It is conceivable that the peak value might be used for model calibration, but in practice its measurement is difficult, and there is also the question of the time necessary to approach a quasi-steady state (cf. Schulkes & Sneyd 1988). The response amplitude M_2 has a similar dependence, with resonance near the critical speed c_{min}.

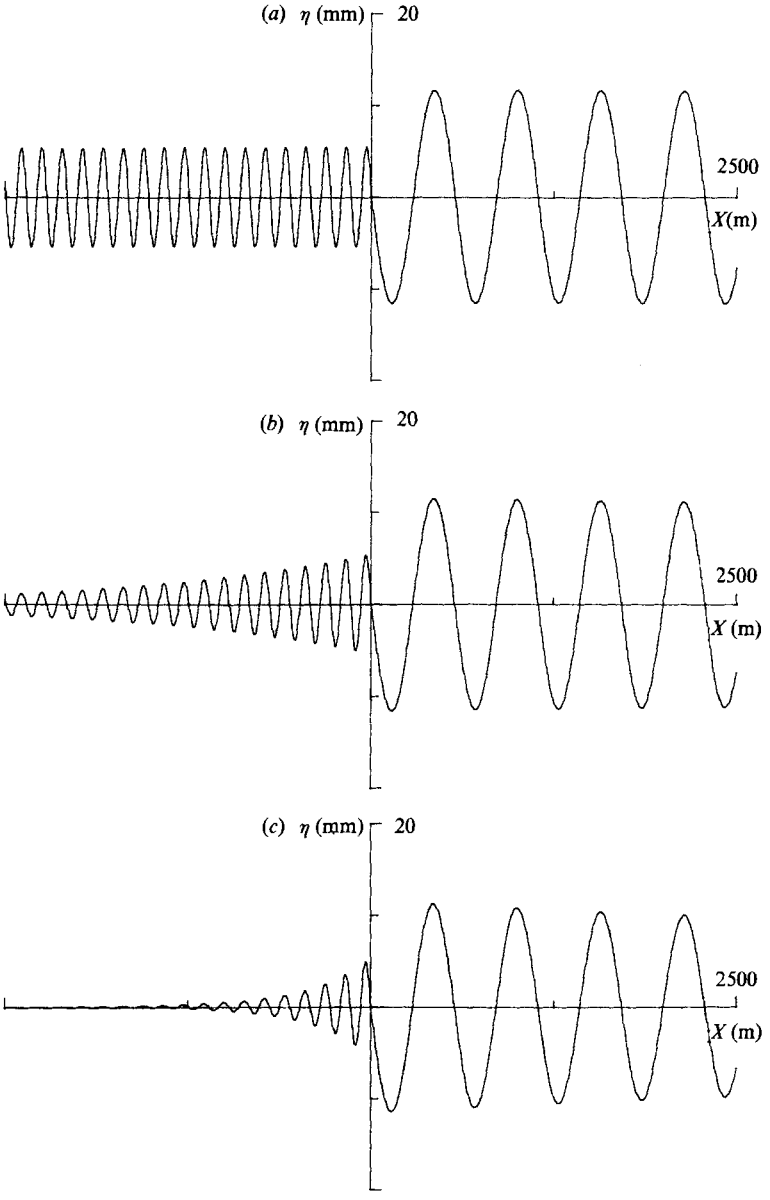

FIGURE 8. Viscoelastic modification of the supercritical response ($V = 30$ m s^{-1}) (*a*) elastic limit; (*b*) $A_0 = 0.05$ s^{-1}, $\alpha_0 = 0.1$ s^{-1}; (*c*) $A_0 = 0.2$ s^{-1}, $\alpha_0 = 0.1$ s^{-1}.

4. Point source

For a steady stress distribution travelling with speed V in the positive x-direction, we write $f(x, y, t) = F(x-Vt, y)$, so that

$$\hat{f}(l, m, \omega) = (2\pi)^{\frac{1}{2}}\delta(Vl-\omega)\,\hat{F}(l, m).$$

In this case Fourier inversion of (2.5) yields

$$\eta(X, y) = -\frac{1}{2\pi}\int_{-\infty}^{\infty}\int_{-\infty}^{\infty}\frac{\hat{F}(l, m)\,\mathrm{e}^{-\mathrm{i}(lX+my)}\,\mathrm{d}l\,\mathrm{d}m}{Dk^4(1-\psi_V)+\rho g-(\rho l^2V^2/k)\coth kH}, \tag{4.1}$$

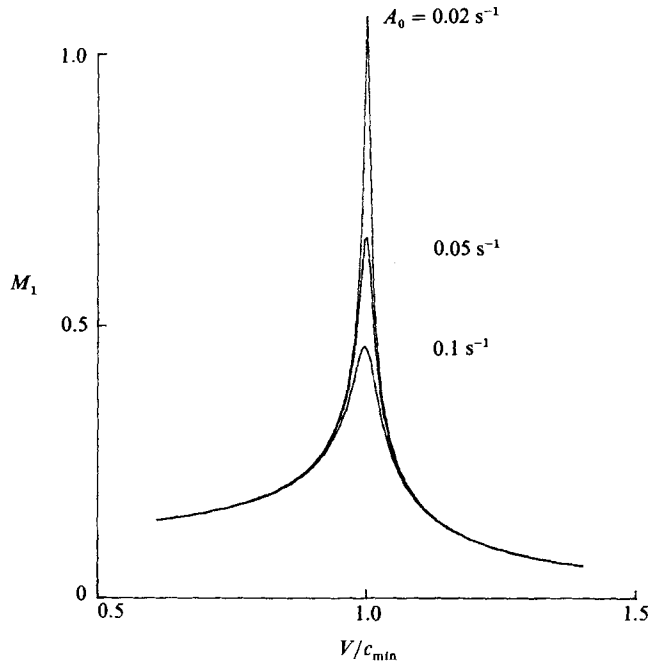

FIGURE 9. Variation of response amplitude with source speed, with A_0 ($\alpha_0 = 0.1\ \mathrm{s}^{-1}$).

where for the memory function $\Psi(t) = A_0 \mathrm{e}^{-\alpha_0 t}$ we have $\psi_V = A_0/(\alpha_0 + \mathrm{i}lV)$. Introducing the same dimensionless variables as in § 3, we can re-express (4.1) as

$$\eta(X) = \frac{-\mathscr{P}}{2\pi} \int\int \frac{\hat{F}(l, m)}{G(l, m)} \mathrm{e}^{-\mathrm{i}(lX+my)}\, \mathrm{d}l\, \mathrm{d}m, \tag{4.2}$$

where $\mathscr{P} = 3/(\rho g L^2)$ and

$$G(l, m) = k^4 - \frac{4l^2V^2}{k} \coth kH + 3 - \frac{\epsilon k^4}{\alpha_0 + \mathrm{i}lV}. \tag{4.3}$$

Note that $G(l, m) = 0$ is the dimensionless viscoelastic dispersion relation with ω replaced by Vl, and the elastic limit corresponds to $\epsilon = 0$ (Davys *et al.* 1985).

4.1. *Steady wave patterns*

We proceed to construct steady wave patterns based on an asymptotic formula for the displacement. In the elastic limit ($\epsilon = 0$) a wavenumber curve is defined by $G(l, m) = 0$ in the (l, m)-plane (cf. Davys *et al.* 1985), but in this viscoelastic theory ($\epsilon \neq 0$) G is complex. Let us write

$$G(\boldsymbol{k}) = B(\boldsymbol{k}) + \mathrm{i}C(\boldsymbol{k}),$$

where B and C now denote its real and imaginary parts, each of which is dependent on the wavenumber $\boldsymbol{k} = (l, m)$ and the viscoelastic parameter ϵ.

If we assume that $\epsilon \ll 1$ (i.e. small viscoelastic dissipation), to order ϵ the complex roots $\boldsymbol{k} = \boldsymbol{k}_\mathrm{R} + \mathrm{i}\boldsymbol{k}_\mathrm{I} (k_\mathrm{I} \ll k_\mathrm{R})$ of $G(\boldsymbol{k}) = 0$ are such that

$$B(\boldsymbol{k}_\mathrm{R}) = 0 \tag{4.4}$$

and

$$\boldsymbol{k}_\mathrm{I} \cdot \nabla B(\boldsymbol{k}_\mathrm{R}) + C(\boldsymbol{k}_\mathrm{R}) = 0. \tag{4.5}$$

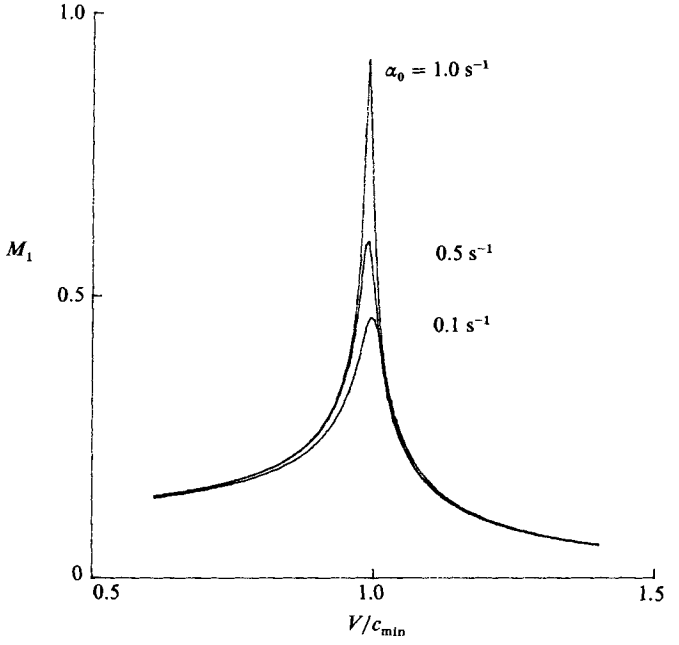

FIGURE 10. Variation of response amplitude with source speed, with α_0 ($A_0 = 0.1\ \mathrm{s}^{-1}$).

Equation (4.4) defines the viscoelastic wavenumber curve $\mathscr{C}_k$, which is the locus of possible $\boldsymbol{k}_\mathrm{R}$ for a steady wave pattern, while (4.5) defines the corresponding $\boldsymbol{k}_\mathrm{I}$, which determines viscoelastic decay. We may solve (4.5) geometrically by drawing another curve $\mathscr{C}_\mathrm{D}$ (the 'damping curve') which is everwhere a normal distance

$$\delta = \left|\frac{C(\boldsymbol{k}_\mathrm{R})}{B_\mathrm{n}(\boldsymbol{k}_\mathrm{R})}\right|$$

inside $\mathscr{C}_k$, where B_n denotes the derivative of B in the normal direction to $\mathscr{C}_k$. As $|\boldsymbol{k}_\mathrm{I}\cdot\nabla B| = \delta|B_n|$, any vector joining a point on the curve $\mathscr{C}_k$ to a neighbouring point on $\mathscr{C}_\mathrm{D}$ will be a solution of (4.5). The viscoelastic curve $\mathscr{C}_k$ is typically close to its elastic limit, and the distance δ to the damping curve $\mathscr{C}_\mathrm{D}$ increases with wavenumber $\boldsymbol{k}$, so as expected shorter waves decay more rapidly than longer waves.

From any point defined by $\boldsymbol{k}_0 = (l_0, m_0)$ on $\mathscr{C}_k$, waves are radiated in the direction of the normal to $\mathscr{C}_k$ at that point (in the sense of increasing ω). Thus the previous dimensional asymptotic formula for the ice displacement at a distance from the load, for waves associated with any such point at which $\mathscr{C}_k$ is convex (cf. equation (3.6) of Davys *et al.* 1985), when modified to include viscoelasticity becomes (Appendix C)

$$\eta \approx \frac{-\hat{F}(\boldsymbol{k}_0)}{B_\mathrm{n}(\boldsymbol{k}_0)}\left(\frac{2\pi}{\kappa_0 r}\right)^{\frac{1}{2}} \mathrm{e}^{-\mathrm{i}(\boldsymbol{k}_0\cdot x+\pi/4-\chi)}\,\mathrm{e}^{-\delta_0 r}, \tag{4.6}$$

which includes the viscoelastic decay factor δ_0 and phase shift χ. Using a point-source approximation to the loading function we replace $\hat{F}(\boldsymbol{k}_0)$ by the constant $\hat{F}(\boldsymbol{0}) = W/2\pi$, where W is the weight of the source. The plot of the viscoelastic decay factor δ_0 in figure 11 clearly shows how much greater it is for shorter waves ahead of the source than for the longer waves behind. We note that the two values of $\delta(\theta)$ at $\theta = 0°$, 180° agree with the values δ_1, δ_2 given by the more restrictive line-load model, cf. figure 7.

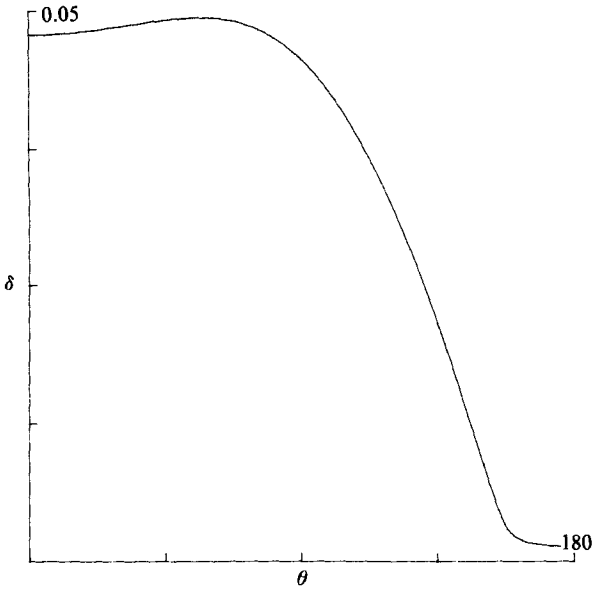

FIGURE 11. Anisotropic viscoelastic decay factor $\delta(\theta)$ for source speed $V = 30$ m s^{-1} and viscoelastic parameters $A_0 = 0.1$ s^{-1}, $\alpha_0 = 0.1$ s^{-1}.

The wave crests are lines of constant phase

$$l_0 X + m_0 y - \chi = K,$$

and to each point P on $\mathscr{C}_k$ there corresponds a point on the wave crest whose polar coordinates in the (x, y)-plane are

$$\left(\frac{K+\chi}{k_0 \cos\gamma}, \theta\right),$$

where $\gamma = \theta - \beta$ and β is the angle between the wavenumber vector $\boldsymbol{k}_0$ and the source velocity (cf. Davys *et al.* 1985). The wave-crest patterns obtained are shown in figure 12, where we observe that the viscoelastic wave crests lag the elastic wave crests but usually only slightly. As V increases towards $V_s = 37.5$ m s^{-1} however – the speed at which caustics form (Davys *et al.* 1985) – the curvature κ of the wavenumber curve becomes locally very small, and the theoretical phase shift χ becomes relatively large. This causes the local disturbances in the wave-crest patterns seen in figure 12, which are particularly noticeable for larger A_0 values. Strictly speaking, the mathematical analysis is invalid if $\chi = O(1)$ but nonetheless should give a correct qualitative picture (cf. also Sneyd 1987).

4.2. *Comparison with Antarctic experiments*

Squire *et al.* (1986) carried out experiments at McMurdo Sound, which provided strainmeter records at various transverse distances (from 30 to 800 m) from an ice road. In figures 13 and 14 we compare two representative ice-strain records, for a strainmeter parallel to the road (at 30 and 100 m respectively), with the responses predicted by elastic and viscoelastic theory. Here we use the physical parameter $D = 1.6 \times 10^9$ Nm determined by Squire *et al.* (1986) for their experiments, for which the critical speed $c_{\min} \approx 18$ m s^{-1}, but retain the viscoelastic parameter values $A_0 = 0.1$ s^{-1}, $\alpha_0 = 0.1$ s^{-1} as shown. The main consequence of viscoelasticity is to

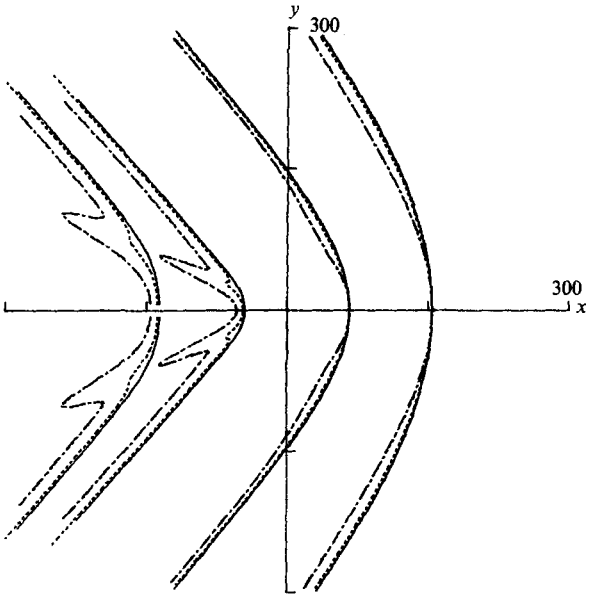

FIGURE 12. Viscoelastic lag of wave pattern, $V = 30$ m s^{-1}. ——, elastic limit; ------, $A_0 = 0.1$ s^{-1}, $\alpha_0 = 0.1$ s^{-1}; ·····, $A_0 = 0.5$ s^{-1}, $\alpha_0 = 0.1$ s^{-1}.

modify the response envelopes, which enhances the quite good agreement between theory and experiment.

The theoretical decay of the maximum response with distance from the source, given by the viscoelastic formula (4.6) as $e^{-\delta_0 r}/r^{\frac{1}{2}}$, is somewhat faster than in the elastic limit (when $\delta_0 = 0$). Squire *et al.* (1986) found that the attenuation is slightly underestimated by the elastic decay.

5. Experiments in Japan

Takizawa (1985, 1986) studied the response of sea ice sheets to moving loads, on Lake Saroma in Japan. In this section we compare results obtained from our viscoelastic model with some of Takizawa's observations that are not so well explained by elastic theory. We use the concentrated line-load theory of §3, for his measurements were made quite near the vehicle path. The parameter values $H = 6.8$ m and $D = 2.0 \times 10^5$ Nm are appropriate for the ice at Lake Saroma, for which the minimum phase speed is $c_{\min} = 6.0$ m s^{-1}. Takizawa found that the maximum depression occurs when the vehicle speed was in the range 5.6 to 6.0 m s^{-1}, so he suggested that it was reasonable to take $c_{min} = 5.8$ m s^{-1}. Our slightly higher value of $c_{\min}$ is consistent with the knowledge that the maximum displacement does not occur exactly at $c_{\min}$ but at a slightly slower speed. The reference timescale T defined in §3 is less than half a second in this case.

Typical ice displacements observed by Takizawa, such as those reproduced in figure 15, correspond to distinctive source-speed regimes (cf. also Eyre 1977; Squire *et al.* 1985, 1986):

(*a*) a quasi-static regime ($V < 0.6 c_{\min}$), when the displacement is similar to that of a static load but the centre of the depression slightly lags the source;

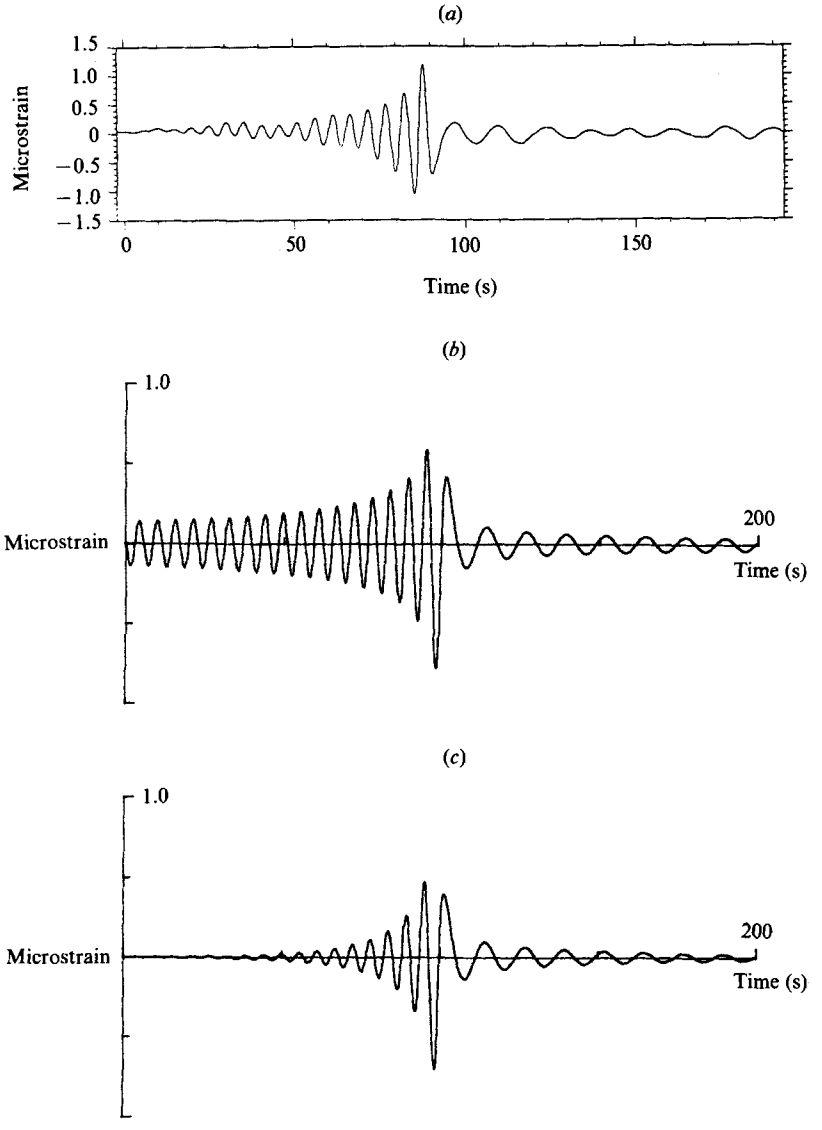

FIGURE 13. Comparison of strainmeter responses for vehicle speed $V = 20.7$ m s^{-1}, at 30 m from test road, (*a*) as observed by Squire *et al.* (1986); (*b*) elastic theoretical; (*c*) viscoelastic theoretical ($A_0 = 0.1$ s^{-1}, $\alpha_0 = 0.1$ s^{-1}).

(*b*) an early-transition regime ($0.6c_{\min} < V < 0.85c_{\min}$), during which the depression becomes narrower and deeper, and the rim rises progressively;

(*c*) a late-transition regime ($0.85c_{\min} < V < c_{\min}$), where a wave-like pattern begins to appear both behind and in front of the source, and simultaneously the depression centre lags behind the source;

(*d*) a two-wave regime ($c_{\min} < V < (gH)^{\frac{1}{2}}$), with a relatively short wave ahead of the source, and a longer wave behind; and

(*e*) a single-wave regime ($V > (gH)^{\frac{1}{2}}$) where the trailing wave disappears, leaving only the shorter wave propagating ahead of the source.

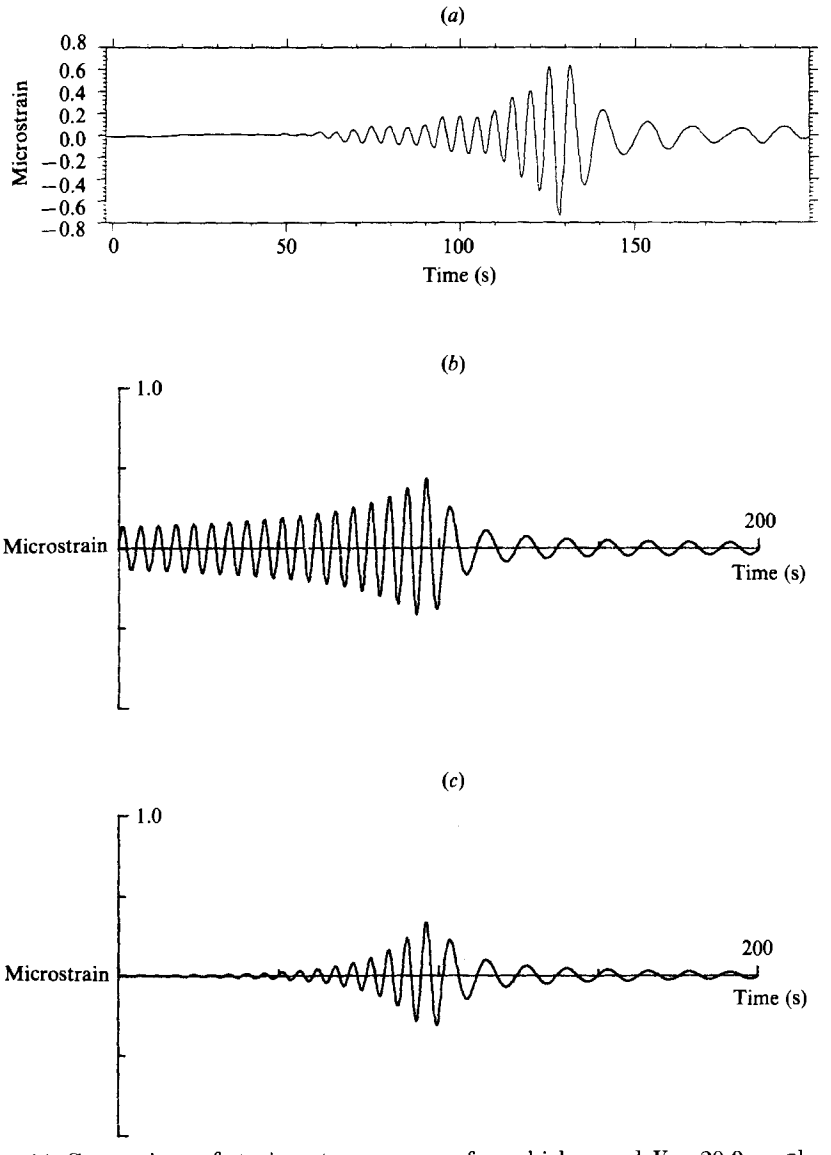

FIGURE 14. Comparison of strainmeter responses for vehicle speed $V = 20.9$ m s^{-1}, at 100 m from text road; (*a*) as observed by Squire *et al.* (1986); (*b*) elastic theoretical; (*c*) viscoelastic theoretical ($A_0 = 0.1$ s^{-1}, $\alpha_0 = 0.1$ s^{-1}).

Figure 16 shows theoretical ice displacement for a representative pair of values for the viscoelastic parameters A_0 and α_0. These theoretical responses have the same characteristics as the experimental results in figure 15, including the lag for slow source speeds not explained by elastic theory. Note that the depression depths are also comparable with the experimental results. As suggested previously, one possible method of estimating the parameters A_0 and α_0 is to compare the theoretical response amplitude M_1 (or M_2) with experimental data, but in Takizawa's experiments the amplitudes are limited by the time the vehicle has been travelling (cf. Schulkes & Sneyd 1988). In so far as the rather qualitative comparison of the displacement

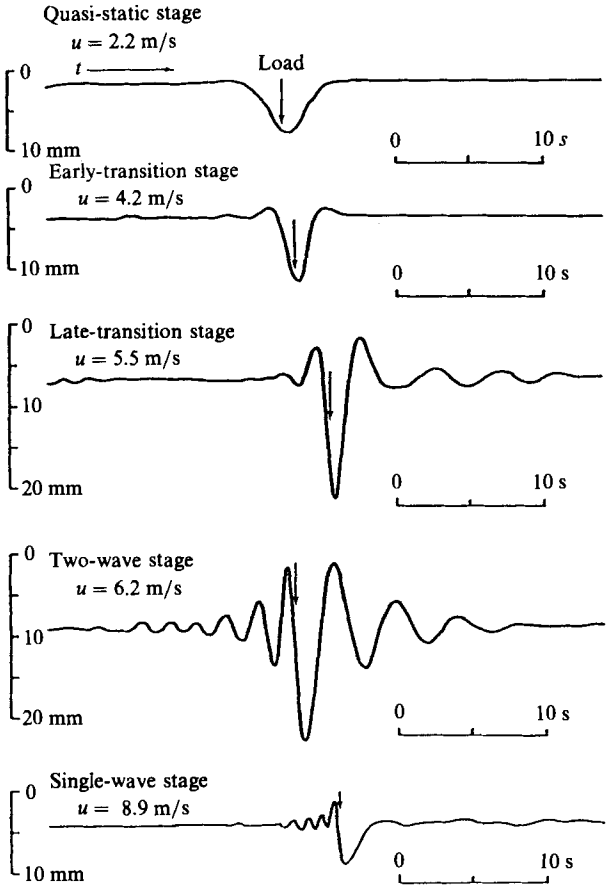

FIGURE 15. Typical observed ice displacement records at various vehicle speeds (from Takizawa 1985).

allows, we assessed A_0 and α_0 to be in the ranges 1.0–2.0 s^{-1} and 1.75–2.0 s^{-1} respectively.

Takizawa noted that the maximum depression lags the source for all speeds however, and that for slow speeds this lag is roughly constant (cf. figure 17). In our viscoelastic model, for fixed A_0 there is only a small range of α_0 such that the lag is almost constant for $V \ll c_{\min}$, so if it is indeed constant we have quite a sensitive test for estimating α_0. The constancy of the lag at low speeds is not so sensitive to the parameter A_0, for fixed α_0. Takizawa observed that the lag for slow speeds was about one metre for observations taken at a distance of one metre from the test track (cf. figure 17). At closer distances the observed lag for slow speeds may be somewhat smaller – perhaps 0.6 m (cf. Takizawa 1985, figure 9). Figure 18 shows the theoretical lag versus speed for various fixed values of A_0, with α_0 in each case determined to produce a constant lag at low speeds. One of these curves corresponds to the viscoelastic parameters for figure 16, and indeed there is an acceptable correlation with the parameter ranges mentioned above.

Takizawa (1985) suggests that the lag time $t_l = lV$ should be comparable with the relaxation time τ of a viscoelastic model. From a graph of t_l versus vehicle speed (cf.

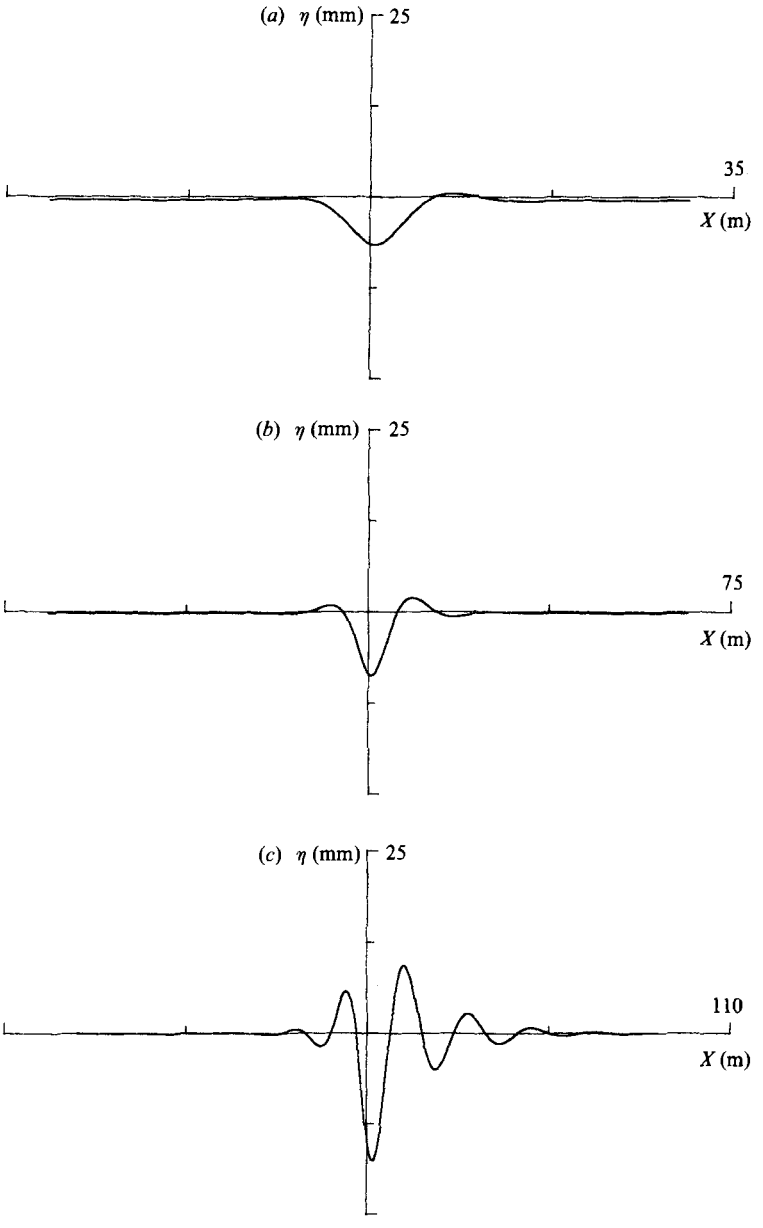

FIGURE 16. Theoretical displacement for comparison with Takizawa (1985). $A_0 = 1.5\ \mathrm{s}^{-1}$, $\alpha_0 = 2.0\ \mathrm{s}^{-1}$. (a) $V = 2.2\ \mathrm{m\ s}^{-1}$, (b) $4.2\ \mathrm{m\ s}^{-1}$, (c) $5.5\ \mathrm{m\ s}^{-1}$.

Takizawa 1985, figure 11) it appears that t_l ranges from 0.2 to 0.8 s. For our viscoelastic model $\tau = \alpha_0^{-1}$, so this suggestion is that α_0 should be in the range 1.25–$5.0\ \mathrm{s}^{-1}$. The values of α_0 we have adopted are certainly within this range.

6. Concluding remarks

A simple memory function with two parameters is adequate to describe the viscoelastic response of a floating ice sheet to a moving vehicle. Typically small

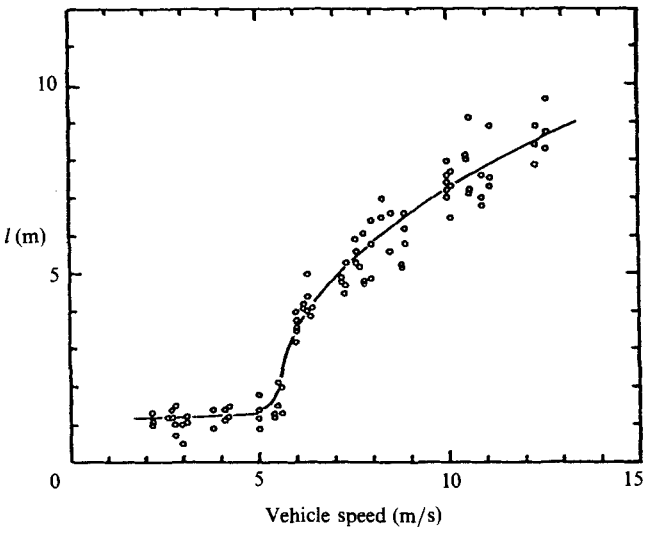

FIGURE 17. Observed variation of lag l, measured at a distance of 1 m, with vehicle speed (from Takizawa 1985).

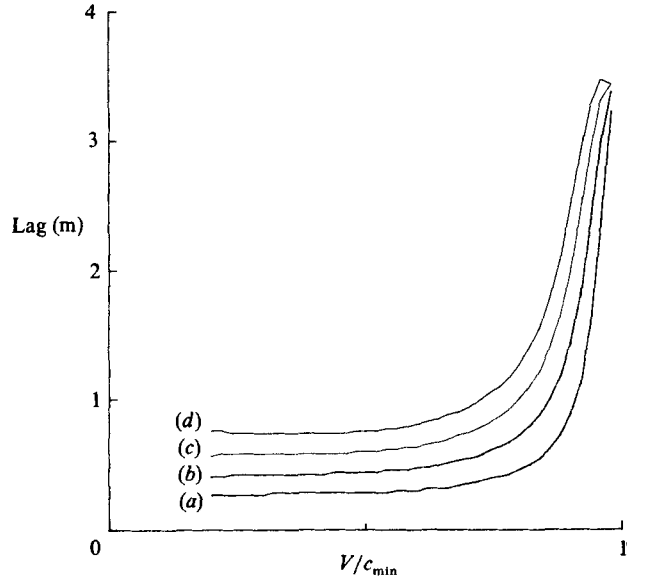

FIGURE 18. Theoretical lag versus source speed, for various pairs of viscoelastic parameters. (*a*) $A_0 = 1.0\ \mathrm{s}^{-1}$, $\alpha_0 = 1.75\ \mathrm{s}^{-1}$; (*b*) $A_0 = 1.5\ \mathrm{s}^{-1}$, $\alpha_0 = 2.0\ \mathrm{s}^{-1}$; (*c*) $A_0 = 2.0\ \mathrm{s}^{-1}$, $\alpha_0 = 2.25\ \mathrm{s}^{-1}$; (*d*) $A_0 = 2.5\ \mathrm{s}^{-1}$, $\alpha_0 = 2.5\ \mathrm{s}^{-1}$.

viscoelastic dissipation produces an asymmetric quasi-static response at subcritical speed ($V < c_{\min}$), renders a finite response at the critical speed $V = c_{\min}$, and damps the shorter leading (elastic) waves more severely than the longer trailing (gravity) waves at supercritical speed ($V > c_{\min}$). The viscoelastic theory can account for the measured lag of the maximum depression immediately behind the load, and generally there is enhanced agreement with experiment for plausible estimates of the two viscoelastic parameters. An asymptotic expression for the ice displacement due

to flexural waves confirms the anisotropic viscoelastic damping with distance from the load, and we also predict an associated wave-crest lag.

We are indebted to our student and colleague R. M. S. M. Schulkes, for his collaboration and enthusiasm during the initial phase of this research.

Appendix A. Proof that viscoelastic parameter $A_0 \geqslant 0$

Consider the case where the displacement is periodic with period $T = 2\pi/\omega$, so the energy dissipation per cycle is approximately

$$\Delta W = \int_0^{2\pi/\omega} \mathrm{Re}\left\{D\nabla^4\left[\eta - \int_0^\infty \Psi(\tau)\,\eta(x, y, t-\tau)\,\mathrm{d}\tau\right]\right\} \mathrm{Re}\{\dot{\eta}\}\,\mathrm{d}t.$$

Writing $\eta(x, y, t) = \eta_0\,\mathrm{e}^{\mathrm{i}(\omega t - \boldsymbol{k}\cdot\boldsymbol{x})}$, we have

$$D\nabla^4\left[\eta - \int_0^\infty \Psi(\tau)\,\eta(x, y, t-\tau)\,\mathrm{d}\tau\right] = D\eta_0 k^4(1-\lambda)\,\mathrm{e}^{\mathrm{i}(\omega t - \boldsymbol{k}\cdot\boldsymbol{x})},$$

where

$$\lambda \equiv \int_0^\infty \Psi(\tau)\,\mathrm{e}^{-\mathrm{i}\omega\tau}\,\mathrm{d}\tau = \frac{A_0}{\alpha_0 + \mathrm{i}\omega}.$$

If we write $1-\lambda = R\,\mathrm{e}^{\mathrm{i}\delta}$, then

$$\begin{aligned}\Delta W &= Dk^4\eta_0^2 R\omega \int_0^{2\pi/\omega} \cos(\boldsymbol{k}\cdot\boldsymbol{x} - \omega t - \delta)\sin(\boldsymbol{k}\cdot\boldsymbol{x} - \omega t)\,\mathrm{d}t,\\ &= \pi Dk^4 R\eta_0^2 \sin\delta.\end{aligned}$$

As energy dissipation must always be positive, it follows that $\sin\delta \geqslant 0$ so $0 \leqslant \delta \leqslant \pi$. Now

$$1-\lambda = \frac{\alpha_0^2 + \omega^2 - \alpha_0 A_0}{\alpha_0^2 + \omega^2} + \mathrm{i}\,\frac{A_0\omega}{\alpha_0^2 + \omega^2},$$

hence

$$R\sin\delta = \frac{A_0\omega}{\alpha_0^2 + \omega^2}.$$

Since R, ω and $\sin\delta$ are all non-negative, so is A_0.

Appendix B. Further analysis of the poles in the integrand of (3.2)

For any function that is meromorphic inside or on a closed curve C in the complex plane

$$N - P = \frac{1}{2\pi}\Delta\arg,$$

where N and P are respectively the number of zeros and poles inside C, and $\Delta\arg$ denotes the change in the argument of the function resulting from a complete traversal of C (see e.g. Titchmarsh 1939, section 3.4). We can use this result to account for all the poles of the integrand of (3.3), treated as a function of the complex variable k: viz.

$$I(k) = \frac{\mathrm{e}^{-\mathrm{i}kX}}{k^4 - 4kV^2\coth kH + 3 - [\epsilon k^4/(\alpha_0 + \mathrm{i}kV)]}.$$

Recall that there are poles at $\pm k_1 - \mathrm{i}\delta_1$, $\pm k_2 + \mathrm{i}\delta_2$, and $\mathrm{i}s_0$; and on the imaginary axis there is also an infinite sequence of poles tending to $\pm \mathrm{i}n\pi/H$ as positive integer

$n \to \infty$. The function $I(k)$ has roots whenever $\coth kH \to \pm\infty$ (i.e. $k = in\pi/H$), or $k = i\alpha_0/V$.

Let us consider a circular contour of large radius on which $k = Re^{i\theta}$, where $0 < \theta < 2\pi$ and $R = (n+\frac{1}{2})\pi/H$, with n large. This choice of radius ensures that none of the previously identified poles lie on the contour $|z| = R$. Then we have $I(k) \approx e^{-ikX}/k^4$, hence $\arg(I(k)) = -RX\cos\theta - 4\theta$ and $\Delta\arg(I(k)) = -8\pi$ for n sufficiently large, so

$$N - P = -4.$$

The contour $|z| = R$ encloses exactly $2n+1$ zeros of $I(k)$, all of them on the imaginary axis, and we have already identified $2n+5$ poles. We therefore conclude that we have identified all the poles.

Appendix C. Asymptotic formula for the displacement

Let us adopt a reference frame moving with the source. Whatever the field direction from the source, we can always orient the axes so that the displacement η far from the source is given by the asymptotic behaviour of (4.1) on $y = 0$ as $x \to \infty$. The inner integral may be evaluated by contour integration. Thus for waves radiating away from the source we seek an asymptotic expression (as $x \to \infty$) for the integral

$$\int_{\mathscr{C}_k} \frac{\hat{F}(l, m)\, e^{-ilx} e^{-\delta x}}{G_l(l, m)}\, dm.$$

arising due to a pole in the complex l-plane with real part $l(m)$ defined by a point on $\mathscr{C}_k$ associated with the direction of propagation, and a small negative imaginary part $-i\delta(m)$ determined from $\mathscr{C}_D$ (we ignore the infinite sequence of poles on the imaginary axis as $x \to \infty$, and the pole near $i\alpha_0/V$).

Since $\delta(m)$ is small and changes only slowly in comparison with $l(m)$, the saddle point at $m_0 = a - i\delta'(a)/l''(a)$ is near the point of stationary phase a (where $l' = 0$) that occurs in the elastic limit. On deforming to a contour of integration passing through m_0 on which $\delta(m) \approx \delta(a)$, and then applying the method of stationary phase, we have the asymptotic expression (4.6) involving the viscoelastic decay factor $\delta(a)$ and a small additional phase shift (Sneyd 1987).

REFERENCES

Bates, H. F. & Shapiro, L. H. 1981*a* Plane waves in a viscoelastic floating ice sheet. *J. Geophys. Res.* **86**(C5), 4263–4723.

Bates, H. F. & Shapiro, L. H. 1981*b* Stress amplification under a moving load on floating ice. *J. Geophys. Res.* **86**(C7), 6638–6642.

Beltaos, S. 1981 Field studies on the response of floating ice sheets to moving loads. *Can. J. Civ. Engng* **8**, 1–8.

Boltzmann, L. 1874 Zur theorie der elastischen nachwirkung. *Sitzber. Akad. Wiss. Wien, Math.-Naturw.* **70**, 275–306.

Coleman, B. D. & Noll, W. 1961 Foundations of linear viscoelasticity. *Rev. Mod. Phys.* **33**, 239–249.

Davys, J. W., Hosking, R. J. & Sneyd, A. D. 1985 Waves due to a steadily moving source on a floating ice plate. *J. Fluid Mech.* **158**, 269–287.

Eyre, D. 1977 The flexural motion of a floating ice sheet induced by moving vehicles. *J. Glaciol.* **19**, 555–570.

Graffi, D. 1982 Mathematical models and waves in linear viscoelasticity. In *Wave Propagation in Viscoelastic Media* (ed. F. Mainardi), pp. 1–27. Pitman.

GREENHILL, A. G. 1887 Wavemotion in hydrodynamics. *Am. J. Maths* **9**, 62–112.

HOSKING, R. J. & SNEYD, A. D. 1986 Waves due to vehicles on floating ice sheets. In *Proc. Ninth Australasian Fluid Mech. Conf., Auckland*, pp. 51–54.

KERR, A. D. 1981 Continuously supported beams and plates subjected to moving loads – a survey. *Solid Mech. Arch.* **6**, 401–449.

KERR, A. D. 1983 The critical velocities of a load moving on a floating ice plate that is subjected to in-plane forces. *Cold Regions Sci. Tech.* **6**, 267–274.

KHEISIN, D. YE. 1963 Moving load on an elastic plate which floats on the surface of an ideal fluid (in Russian). *Izv. Akad. Nauk SSSR, Otd. Tekh. Nauk Mekh. Mashinostr.* **1**, 178–180.

SCHULKES, R. M. S. M., HOSKING R. J. & SNEYD, A. D. 1987 Waves due to a steadily moving source on a floating ice plate. Part 2. *J. Fluid Mech.* **180**, 297–318.

SCHULKES, R. M. S. M. & SNEYD, A. D. 1988 Time-dependent response of a floating ice sheet to a steadily moving load. *J. Fluid Mech.* **186**, 25–46.

SNEYD, A. D. 1987 Effect of dissipation on waves due to a steadily moving source. *University of Waikato Res. Rep.* 152.

SQUIRE, V. A. & ALLAN, A. J. 1980 Propagation of flexural gravity waves in sea ice. In *Sea Ice Processes and Models* (ed. R. S. Pritchard), pp. 327–338. University of Washington Press, Seattle and London.

SQUIRE, V. A., LANGHORNE, P. J., ROBINSON, W. H. & HEINE, A. J. 1986 KIWI 131 – an Antarctic field experiment to study strains and acoustic emission generated by loads moving over sea ice. Report for the Royal Society of London.

SQUIRE, V. A., ROBINSON, W. H., HASKELL, T. G. & MOORE, S. G. 1985 Dynamic strain response of lake and sea ice to moving loads. *Cold Regions Sci. Tech.* **11**, 123–139.

TABATA, T. 1958 Studies on viscoelastic properties of sea ice. In *Arctic Sea Ice*. US National Academy of Sciences & National Research Council (Washington, DC), publication 598, pp. 139–147.

TAKIZAWA, T. 1985 Deflection of a floating sea ice sheet induced by a moving load. *Cold Regions Sci. Tech.* **11**, 171–180.

TAKIZAWA, T. 1986 Response of a floating sea ice sheet to a moving vehicle. In *Proc. Fifth International Offshore Mechanics and Arctic Engineering Symposium, Tokyo*; vol. 4, pp. 614–621.

TITCHMARSH, E. C. 1939 *The Theory of Functions*. Oxford University Press.

WILSON, J. T. 1958 Moving loads on floating ice sheets. *Project* 2432. University of Michigan Research Institute.